NASA TECHNICAL MEMORANDUM

NASA TM X-3291

NASA TM X-3291

SURFACE RECESSION CHARACTERISTICS OF A CRYOGENIC INSULATION SUBJECTED TO ARC-TUNNEL HEATING

Claud M. Pittman and Ronald D. Brown

Langley Research Center
Hampton, Va. 23665

NATIONAL AERONAUTICS AND SPACE ADMINISTRATION • WASHINGTON, D. C. • NOVEMBER 1975

1. Report No. NASA TM X-3291	2. Government Accession No.	3. Recipient's Catalog No.
4. Title and Subtitle SURFACE RECESSION CHARACTERISTICS OF A CRYOGENIC INSULATION SUBJECTED TO ARC-TUNNEL HEATING		5. Report Date November 1975 6. Performing Organization Code
7. Author(s) Claud M. Pittman and Ronald D. Brown		8. Performing Organization Report No. L-10371
9. Performing Organization Name and Address NASA Langley Research Center Hampton, Va. 23665		10. Work Unit No. 506-16-43-02 11. Contract or Grant No.
12. Sponsoring Agency Name and Address National Aeronautics and Space Administration Washington, D.C. 20546		13. Type of Report and Period Covered Technical Memorandum 14. Sponsoring Agency Code
15. Supplementary Notes		

16. Abstract

Specimens of a cryogenic insulation, proposed for use on the space shuttle external tank, were tested in an arc tunnel over a range of heating rates, pressures, and enthalpies corresponding to the shuttle ascent environment. A regression analysis was used to correlate the test data. Correlation equations involving surface recession rate as a function of heating rate, pressure, and enthalpy were developed. These equations can be used to make total surface recession predictions for shuttle ascent flight environments.

17. Key Words (Suggested by Author(s))	18. Distribution Statement
Spray-on foam insulation Cryogenic insulation Surface recession	Unclassified – Unlimited Subject Category 27

19. Security Classif. (of this report)	20. Security Classif. (of this page)	21. No. of Pages	22. Price*
Unclassified	Unclassified	28	$3.75

*For sale by the National Technical Information Service, Springfield, Virginia 22161

SURFACE RECESSION CHARACTERISTICS OF A CRYOGENIC INSULATION SUBJECTED TO ARC-TUNNEL HEATING

Claud M. Pittman and Ronald D. Brown
Langley Research Center

SUMMARY

Specimens of a cryogenic insulation, proposed for use on the space shuttle external tank, were tested in an arc tunnel over a range of heating rates, pressures, and enthalpies corresponding to the shuttle ascent environment. A regression analysis was used to correlate the test data. Correlation equations involving surface recession rate as a function of heating rate, pressure, and enthalpy were developed. These equations can be used to make total surface recession predictions for shuttle ascent flight environments.

INTRODUCTION

Polyurethane foam has been used as cryogenic insulation on the liquid hydrogen tanks of launch vehicles. A polyurethane foam which was used on the Saturn S-II (ref. 1) is being considered for application on the space shuttle external tank. This application introduces a new aspect in the use of the cryogenic insulation because the material is applied to the exterior of the tank and is, therefore, subjected to aerodynamic heating.

The present tank design requires a layer of cryogenic insulation over both the liquid hydrogen and liquid oxygen portions of the external tank to reduce the probability of ice and frost formation which increases vehicle weight. Therefore, the foam will be subjected to both mild and severe ascent heating conditions. Because both weight and cost can be saved if the cryogenic insulation can accommodate a significant part of the thermal protection requirements, the ablation characteristics of the foam must be determined so that the foam can be a part of the heat shield design. Furthermore, since the foam is an excellent insulator, the surface recession characteristics of the material are the most significant design variable.

In this paper, surface recession data from a series of arc-tunnel tests of cryogenic insulation specimens are presented. In these tests, the heating rate was varied from 7.95 to 238 kW/m^2 (0.7 to 21 Btu/ft^2-sec), the pressure from 0.0011 to 0.8 atm (1 atm = 101.3 kPa), and the enthalpy from 1.32 to 9.65 MJ/kg (570 to 4160 Btu/lb). An equation which correlates the surface recession data was developed.

SYMBOLS

Values are given in both SI and U.S. Customary Units. The measurements and calculations were made in U.S. Customary Units.

a,b,c	exponential factors (eq. (4))
C	constant (eq. (4))
H	total enthalpy, J/kg (Btu/lb)
H_w	cold-wall enthalpy at 294 K (70^o F), J/kg (Btu/lb)
l	length, cm (in.)
p	local pressure at the surface, atm
p_t	stagnation pressure, atm
q	cold-wall heating rate, W/m^2 (Btu/ft^2-sec)
R	recession rate, cm/sec (in/sec)
r_n	nose radius, cm (in.)
t	thickness, cm (in.)
Δx	recession, cm (in.)

Subscripts:

calc	calculated
exp	experimental

SPACE SHUTTLE EXTERNAL TANK

Configuration

The space shuttle external tank configuration is shown in figure 1. The liquid oxygen (LO_2) tank is located in the forward section and the liquid hydrogen (LH_2) tank is in

the aft section. The maximum heating rate point on the liquid oxygen tank is indicated. The present thermal protection system design for the external tank requires a layer of cryogenic insulation over the entire tank to reduce the probability of ice and frost formation during ground hold.

Flight Environment

A typical flight environment at the maximum heating rate point on the liquid oxygen portion of the external tank is shown in figure 2. The first 200 seconds of the trajectory produce a very severe ascent environment. The heating rate and surface pressure are high and the enthalpy is low. During the last 400 seconds of the ascent trajectory (separation occurs soon after 600 seconds), the environment is much milder. The heating rate and surface pressure are low and the enthalpy is high.

On the liquid hydrogen portion of the tank, the flight environment is much less severe except for special areas where interference effects, due to the orbiter, produce an environment similar to that shown in figure 2.

ARC-TUNNEL TESTS

Material

The polyurethane foam used in these tests is specifically formulated for spray application. After application, the material has a density of about 32 kg/m^3 (2 lb/ft^3). Some of the test material had a vinyl coating which was applied to reduce handling damage.

Test Specimens

The specimens used in the tests were 12.7 cm (5 in.) square and 2.54 cm (1 in.) thick. The specimens were mounted on the side of a water-cooled wedge test fixture as shown in figure 3. The first 15 specimens had a 30-gage chromel-alumel thermocouple inserted in the center of the back surface of the specimen to a location 0.63 cm (0.25 in.) from the front surface. Eight of the first 15 specimens had a protective vinyl coating on the front surface. None of the other specimens were coated.

Test Environments

The arc tunnel used for these tests is described in reference 2. The test specimens were exposed to the environments listed in tables I and II. The test stream was air. Cold-wall heating rates, heating rate distributions, and surface pressures were determined by using calibration models of the same size and shape as the specimens. Thin-skin calorimeters were used for the heating rate measurements. Specimens 1 to 52 were tested in supersonic flow. Specimens 53, 54, and 55 were tested in subsonic flow.

Except for the subsonic tests (specimens 53, 54, and 55), the test stream enthalpies were determined by using an established facility procedure. Probes were used to determine the stagnation heating rate and stagnation pressure in the center of the stream. A correlation equation was then used to calculate the enthalpy. Enthalpies determined by this method agree well with enthalpies calculated by energy balance methods.

The correlation equation used with the measured heating rate and pressure is

$$\frac{q\sqrt{r_n}}{(H - H_w)\sqrt{p_t}} = 0.113 \frac{kg}{m^{1.5}\text{-sec-atm}^{0.5}} \left(0.042 \frac{lb}{ft^{1.5}\text{-sec-atm}^{0.5}}\right) \tag{1}$$

where r_n is the hemispherical radius of the heating rate probe (1.9 cm (0.75 in.)), H_w is the enthalpy at room temperature (294 K (70° F)), and p_t is the stagnation pressure in the stream. The high enthalpy—low pressure tests (the first 15 specimens, see table I) were conducted with the specimen at a 2° angle of attack. This angle of attack was selected to obtain the desired heating environment. In these tests, the environmental parameters correlated with the following equation:

$$\frac{q\sqrt{l}}{(H - H_w)\sqrt{p}} = 0.059 \frac{kg}{m^{1.5}\text{-sec-atm}^{0.5}} \left(0.022 \frac{lb}{ft^{1.5}\text{-sec-atm}^{0.5}}\right) \tag{2}$$

where q is the measured heating rate at the center of the thin-skin calorimeter, l is the distance from the leading edge of the wedge to the center of the specimen (15 cm (6 in.)), H is the calculated enthalpy, and p is the static pressure at the center of the model.

In the low enthalpy—high pressure tests (table II), the specimens were at a 32° angle of attack. In these tests the environmental parameter correlation equation is

$$\frac{q\sqrt{l}}{(H - H_w)\sqrt{p}} = 0.103 \frac{kg}{m^{1.5}\text{-sec-atm}^{0.5}} \left(0.038 \frac{lb}{ft^{1.5}\text{-sec-atm}^{0.5}}\right) \tag{3}$$

Although the flight environment heating rates could be simulated in the supersonic flow tests, the test pressures were generally too low and the test enthalpy too high to provide an accurate simulation of the first part of the ascent environment. To obtain a good supersonic flow simulation of all three parameters would have required higher mass flow in the tunnel. A higher mass flow at the required power settings "blows out" the arc and the facility will not operate.

A typical heating rate distribution for the high enthalpy (2° angle of attack) tests is shown schematically in figure 4. The locations of the thermocouples, which were attached to the underside of the skin, are shown. No thermocouple was attached at the center point of the calorimeter. The heating rate at the center point was taken as the average of the

two adjacent heating rates. All heating rate values were normalized to the center point. All heating rate values given in the tables are for the center location.

A typical heating rate distribution for the supersonic tests with low enthalpy and a 32° angle of attack is shown in figure 5. The locations of the thermocouples are given.

The pressure port locations on the pressure calibration model are shown in figure 6 and typical pressure distributions, normalized to the center point, are given for both the high and low enthalpy tests. The pressure values, given in the tables, are for the center location.

As was mentioned previously, surface pressures high enough to simulate flight pressures during the initial part of the trajectory could not be obtained with supersonic flow. As will be shown later, some high pressure data were required. Therefore, specimens 53, 54, and 55 were tested in subsonic flow. In these tests, the heating rates and pressures did not vary significantly over the surface of the specimens. The enthalpy for these tests was obtained by using an arc-heater energy balance.

Test Procedure

Tunnel operating conditions were established, and the test environment was allowed to stabilize. Heating rate and pressure measurements were made. The specimen was inserted into the stream and exposed to the test environment, either until the temperature at the thermocouple location increased 167 K (300° F) (high enthalpy tests) or for a predetermined time (low enthalpy tests). The specimen was removed from the stream and posttest heating rate and pressure measurements were made. Pretest and posttest measurements were essentially the same.

By terminating the high enthalpy tests when the temperature rise at the thermocouple location was 167 K (300° F), surface recession at the center point was limited to about 0.7 cm (0.27 in.). The data from reference 2 indicate that the test specimen surface environment at the center point probably did not change significantly with this thickness change.

In the low enthalpy tests, a more complete investigation was made for each of the three major test conditions. (See table II.) At each test condition, duplicate tests and tests at progressively longer test times were made to determine if material variations and specimen shape change significantly affected surface recession rates. The time each specimen was exposed to the stream was controlled by an automatic timer.

RESULTS AND DISCUSSION

The test results are given in the tables. The time each specimen was exposed to the stream, the recession at the center point of each specimen, and the recession rate at the

center point of each specimen are given. Figure 7 shows the final shape of a typical model after testing. The specimen shown in the figure had a total recession of about 0.5 cm (0.2 in.) at the center point. No significant changes in specimen profile across the model were evident.

High Enthalpy Tests

The data for the high enthalpy tests (table I) show that, at low pressure, surface recession of the cryogenic insulation starts at a heating rate of about 10 to 11 kW/m^2 (0.88 to 1.0 Btu/ft^2-sec). This heating rate level corresponds to a surface radiation equilibrium temperature of about 700 K (800° F) (assuming an emittance of 0.8). The surfaces of the first three specimens were darker after heating, indicating that some pyrolysis had occurred. Some intumescence was also evident in these specimens.

Specimens 4 to 12 had progressively darker surfaces and progressively thinner degraded surface layers (about 0.5 cm (0.2 in.) on specimen 4, about 0.05 cm (0.02 in.) on specimen 12). The degraded layer was not a typical rigid, carbonaceous char, but was ductile and resilient. None of the remaining specimens showed any evidence of a char layer. The maximum surface temperature of these specimens was probably less than that of the specimens just discussed.

Recession rate data for specimens 4 to 15 are plotted as a function of heating rate in figure 8. The data show that the coating on the eight coated specimens had no significant effect on the recession rate.

Low Enthalpy Tests

Three primary test conditions were used for the low enthalpy, high pressure tests. At each test condition, duplicate specimens were tested for progressively longer test times. Except for the very short time tests, which showed a transient period when the recession rate increased, the recession rate showed very little, if any, time dependence. (Note the test results for specimens 18 to 27, 30 to 41, and 44 to 51 given in table II.) Thus, there was no evidence that the surface heating environment changed significantly as the specimen shape changed.

Visual observations of both the specimens and the tests indicate that differences between recession rates of duplicate specimens were more likely due to variations in the material rather than in the test conditions. Density variations between specimens were as much as 10 percent and thin, high density skins at various depths, formed between spray passes during specimen fabrication, affected recession rates of some specimens. None of the specimens showed any evidence of a char layer.

One specimen (number 52) was tested under very severe heating rate and pressure conditions. The test time for this specimen was short and the recession was large.

Although it may have been fortuitous, this datum point correlated well with the other low enthalpy test results.

The low enthalpy specimen recession rates are plotted against heating rate in figure 9. The curve was drawn through the center of clustered data points. Most of the points at some distance from the line were data from short time tests in which transient effects produced low recession rates. The data from the subsonic tests are also shown in the figure. These data will be discussed later.

Data Correlation

The curves from the overlapping heating rate range of figures 8 and 9 are shown in figure 10. Note that the recession rates from the low enthalpy tests are always larger than the recession rates from the high enthalpy tests; but in the low enthalpy tests, the recession rate increases less rapidly with heating rate.

A regression analysis was used to correlate the supersonic flow data from both sets of tests. An equation of the form

$$R = Cq^{a}p^{b}H^{c} \tag{4}$$

was assumed. Equation (4) was linearized using logarithms. Enthalpy was included as an independent variable even though enthalpy was calculated from the stagnation heating rate and pressure. The rationale for including enthalpy is that the environmental parameter equations (eqs. (2) and (3)) are different for the two angles of attack used and that enthalpy is a prime descriptor of the flight environment.

Forty-five data points were included in the regression analysis. The first three data points were excluded because no recession occurred in these tests. Data from specimens 16, 17, 28, and 29 were excluded because transient effects were, in general, significant in these short time tests.

The equation resulting from the regression analysis was

In cm/sec:

$$R = 0.96q^{0.315}p^{1.336}H^{1.2}$$

In in/sec:

$$R = 6.02 \times 10^{-4}q^{0.315}p^{1.336}H^{1.2}$$

(5)

Figure 11 shows recession rates calculated with this equation plotted against the experimental recession rate data. The equation gives a good correlation of all the supersonic flow data. However, the exponents obtained in equations (5) were unexpected. From figures 8 and 9, a much stronger heating rate dependence was expected and none of the data indicated the strong pressure dependence shown in the equations. Furthermore, both the data and ablation theory (ref. 3) show that the recession rate should be inversely proportional to the enthalpy.

Equations (5) were used to calculate total recession for the ascent trajectory given in figure 2. Ten-second time steps were used for the integration. The flight heating rate was corrected for the difference in cold-wall conditions between flight and ground test. The expression used was

$$q = q_{\text{flight}} \frac{\left(H - H_{294\ K}\right)}{\left(H - H_{255\ K}\right)} = q_{\text{flight}} \frac{\left(H - H_{70^{\circ}\ F}\right)}{\left(H - H_{0^{\circ}\ F}\right)}$$

The recession, calculated with equations (5), is shown as a function of ascent trajectory time in figure 12. Total recession was very large, 51.5 cm (20 in.). Nearly 90 percent of the total recession occurred during the first 110 seconds when the local pressure in flight was much higher than the ground test pressures and the flight enthalpy was lower. The high pressure caused the very high calculated recession during the first 110 seconds of the trajectory. Equations (5) had evidently been extrapolated to pressure levels at which the equations were not valid.

Because of the unrealistic results obtained through the use of equations (5), specimens 53, 54, and 55 were tested in the subsonic flow test conditions given in table II. When these three data points were included in the regression analysis, the following equations (with 48 data points) were obtained:

In cm/sec:

$$R = 6.04 \times 10^{-5} q^{1.88} p^{0.16} H^{-0.442}$$

In in/sec:

$$R = 0.334 q^{1.88} p^{0.16} H^{-0.442} \qquad (6)$$

The data correlation obtained with equations (6) is shown in figure 13. The correlation is good; however, the errors at all recession rates are of the same order of magnitude. Since most of the total recession occurs at the higher recession rates, reducing the error at high recession rates at the expense of increasing the error at low recession rates was

desirable. This was done by weighting each data point by a number equal to the recession rate squared. The resulting equations were

In cm/sec:

$$R = 7.45 \times 10^{-4} q^{1.306} p^{0.123} H^{-0.3877}$$

In in/sec:

$$R = 0.0735 q^{1.306} p^{0.123} H^{-0.3877} \qquad (7)$$

The data correlation obtained with equations (7) is shown in figure 14.

An examination of figure 14 shows that a better correlation could be obtained by subtracting a constant in equations (7). The resulting equation (with the constant chosen somewhat arbitrarily) was

In cm/sec:

$$R = 7.45 \times 10^{-4} q^{1.306} p^{0.123} H^{-0.3877} - 0.005$$

In in/sec:

$$R = 0.0735 q^{1.306} p^{0.123} H^{-0.3877} - 0.00197 \qquad (8)$$

The data correlation obtained with equations (8) is shown in figure 15.

The trajectory shown in figure 2 was used in equations (6), (7), and (8) to calculate recession as a function of time. The results are shown in figure 16. Total recession was only 25 percent of the recession given by equations (5). Recession calculated by equations (7) was about 10 percent more than that calculated by equations (6) and (8). The difference in recession occurred when the recession rate became less than about 0.07 cm/sec (0.028 in/sec). From the correlation of equations (6) (fig. 13), calculated recession rates were, in general, less than or equal to experimental rates at the lower values. In the correlation of equations (7) (fig. 14), the reverse is true. This difference caused the increase in total recession given by equations (7).

Equations (6) and (8) gave nearly identical recession rates throughout the trajectory. When using equations (8), the recession rate was assumed to be zero when the rate became negative.

CONCLUDING REMARKS

Specimens of a cryogenic insulation, proposed for use on the space shuttle external tank, were tested in an arc tunnel over a range of heating rates, pressures, and enthalpies. The heating rate range corresponded very well with the heating rates expected in flight. However, the test pressures were too low and the test enthalpies too high to simulate the initial ascent heat pulse. The pressure and enthalpy mismatch was reversed for the last part of the flight environment, but material recession rates are relatively small in this latter environment.

A regression analysis was used to obtain a data correlation equation which gave surface recession as a function of heating rate, pressure, and enthalpy. This correlation equation had a theoretically unexpected enthalpy dependence and a strong pressure dependence that was not apparent from a close examination of the test results. When this equation was used with the flight trajectory, a very large total recession was obtained. The correlation equation had evidently been extrapolated to conditions where it was no longer valid. Therefore, additional data were obtained in a high pressure, arc-tunnel environment and satisfactory correlation equations were obtained.

Langley Research Center
National Aeronautics and Space Administration
Hampton, Va. 23665
September 25, 1975

REFERENCES

1. Mack, F. E.; and Smith, M. E.: High-Performance Spray-Foam Insulation for Application on Saturn S-II Stage. Advances in Cryogenic Engineering, Volume 16, K. D. Timmerhaus, ed., Plenum Press, 1971, pp. 118-127.

2. Brown, Ronald D.; and Jakubowski, Antoni K.: Heat-Transfer and Pressure Distributions for Laminar Separated Flows Downstream of Rearward-Facing Steps With and Without Mass Suction. NASA TN D-7430, 1974.

3. Roberts, Leonard: A Theoretical Study of Stagnation-Point Ablation. NASA TR R-9, 1959. (Supersedes NACA TN 4392.)

TABLE I.- HIGH ENTHALPY TEST CONDITIONS AND RESULTS

Specimen	q		p, atm	H		Time, sec	Δx		R	
	kW/m^2	Btu/ft^2-sec		MJ/kg	Btu/lb		cm	in.	cm/sec	in/sec
1	7.95	0.70	0.00110	2.64	1140	140	----	----	------	-------
2	9.99	.88	.00113	2.88	1240	115	----	----	------	-------
[a] 3	9.99	.88	.00113	2.88	1240	135	----	----	------	-------
4	11.35	1.00	.00120	3.06	1320	87	0.051	0.020	0.00058	0.000231
5	12.49	1.10	.00123	3.27	1410	49	.076	.030	.00155	.000611
6	13.62	1.20	.00125	3.55	1530	85	.102	.040	.00119	.000472
[a] 7	13.62	1.20	.00125	3.55	1530	93	.107	.042	.00114	.000453
[a] 8	15.89	1.40	.00130	3.92	1690	68	.132	.052	.00193	.000764
[a] 9	19.30	1.70	.00143	4.27	1840	74	.254	.100	.00343	.00135
10	22.70	2.00	.00190	5.38	2320	57	.206	.081	.00361	.00142
[a] 11	22.70	2.00	.00190	5.38	2320	50	.163	.064	.00325	.00128
12	49.94	4.4	.00260	9.65	4160	29	.533	.210	.0183	.00723
[a] 13	65.83	5.8	.00470	7.75	3340	14	.721	.283	.0516	.0202
[a] 14	79.45	7.0	.00960	5.10	2200	15	.859	.338	.0584	.0225
[a] 15	113.5	10.0	.00950	7.66	3300	10	.828	.325	.0828	.0325

[a] Coated specimens.

TABLE II.- LOW ENTHALPY TEST CONDITIONS AND RESULTS

Specimen	q		p, atm	H		Time, sec	Δx		R	
	kW/m^2	Btu/ft^2-sec		MJ/kg	Btu/lb		cm	in.	cm/sec	in/sec
16	48.8	4.3	0.0351	1.32	570	1.5	0.066	0.026	0.0439	0.0173
17	↓	↓	↓	↓	↓	1.6	.046	.018	.0286	.0113
18	↓	↓	↓	↓	↓	3.05	.193	.076	.0635	.0249
19	↓	↓	↓	↓	↓	3.2	.122	.048	.0381	.0150
20	↓	↓	↓	↓	↓	3.9	.132	.052	.0356	.0130
21	↓	↓	↓	↓	↓	4.0	.251	.099	.0630	.025
22	↓	↓	↓	↓	↓	5.2	.290	.114	.0559	.022
23	↓	↓	↓	↓	↓	5.25	.318	.125	.0604	.024
24	↓	↓	↓	↓	↓	6.5	.381	.150	.0584	.023
25	↓	↓	↓	↓	↓	6.7	.467	.184	.0700	.027
26	↓	↓	↓	↓	↓	7.4	.465	.183	.0627	.025
27	↓	↓	↓	↓	↓	7.8	.500	.197	.0643	.025
28	88.5	7.8	.0543	1.69	730	1.6	.160	.063	.100	.039
29	↓	↓	↓	↓	↓	1.6	.221	.087	.138	.054
30	↓	↓	↓	↓	↓	2.1	.284	.112	.135	.053
31	↓	↓	↓	↓	↓	2.1	.262	.103	.124	.049
32	↓	↓	↓	↓	↓	2.55	.376	.148	.147	.058
33	↓	↓	↓	↓	↓	2.55	.378	.149	.148	.058
34	↓	↓	↓	↓	↓	3.05	.445	.175	.146	.057
35	↓	↓	↓	↓	↓	3.05	.462	.181	.152	.060
36	↓	↓	↓	↓	↓	3.5	.554	.218	.158	.062
37	↓	↓	↓	↓	↓	3.5	.544	.214	.155	.061
38	↓	↓	↓	↓	↓	4.0	.574	.240	.144	.060
39	↓	↓	↓	↓	↓	4.0	.610	.226	.152	.056
40	↓	↓	↓	↓	↓	4.5	.683	.269	.135	.050
41	↓	↓	↓	↓	↓	4.5	.610	.226	.135	.050
42	131	11.5	.0693	1.81	780	1.1	.264	.104	.240	.094
43	↓	↓	↓	↓	↓	1.1	.244	.096	.222	.087
44	↓	↓	↓	↓	↓	1.6	.445	.175	.278	.109
45	↓	↓	↓	↓	↓	1.6	.406	.160	.254	.100
46	↓	↓	↓	↓	↓	2.1	.566	.222	.270	.106
47	↓	↓	↓	↓	↓	2.1	.584	.230	.278	.109
48	↓	↓	↓	↓	↓	2.55	.589	.232	.231	.091
49	↓	↓	↓	↓	↓	2.55	.665	.262	.261	.103
50	↓	↓	↓	↓	↓	3.05	.668	.263	.219	.086
51	↓	↓	↓	↓	↓	3.05	.859	.338	.281	.110
52	238	21	.100	1.97	850	1.5	.787	.310	.526	.207
[a]53	100	8.8	.80	↓	↓	2.0	.427	.168	.213	.084
[a]54	↓	↓	↓	↓	↓	2.5	.508	.200	.203	.080
[a]55	↓	↓	↓	↓	↓	3.0	.762	.300	.254	.100

[a]Subsonic flow.

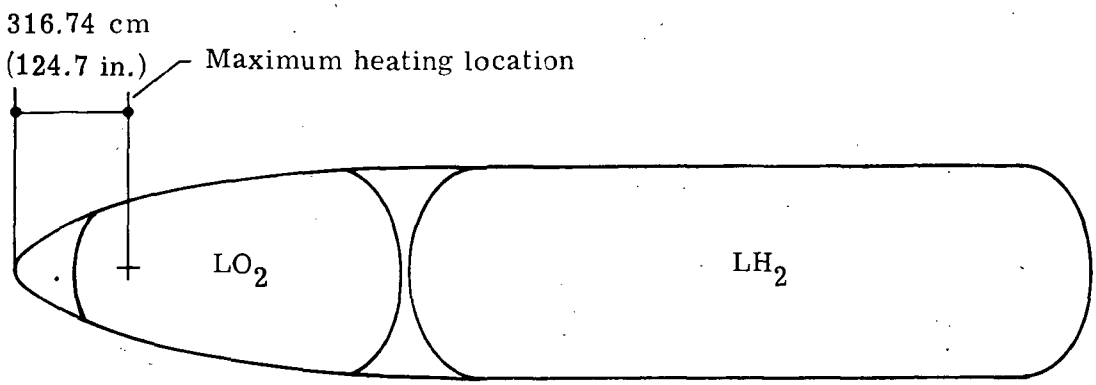

Figure 1.- Shuttle external tank configuration.

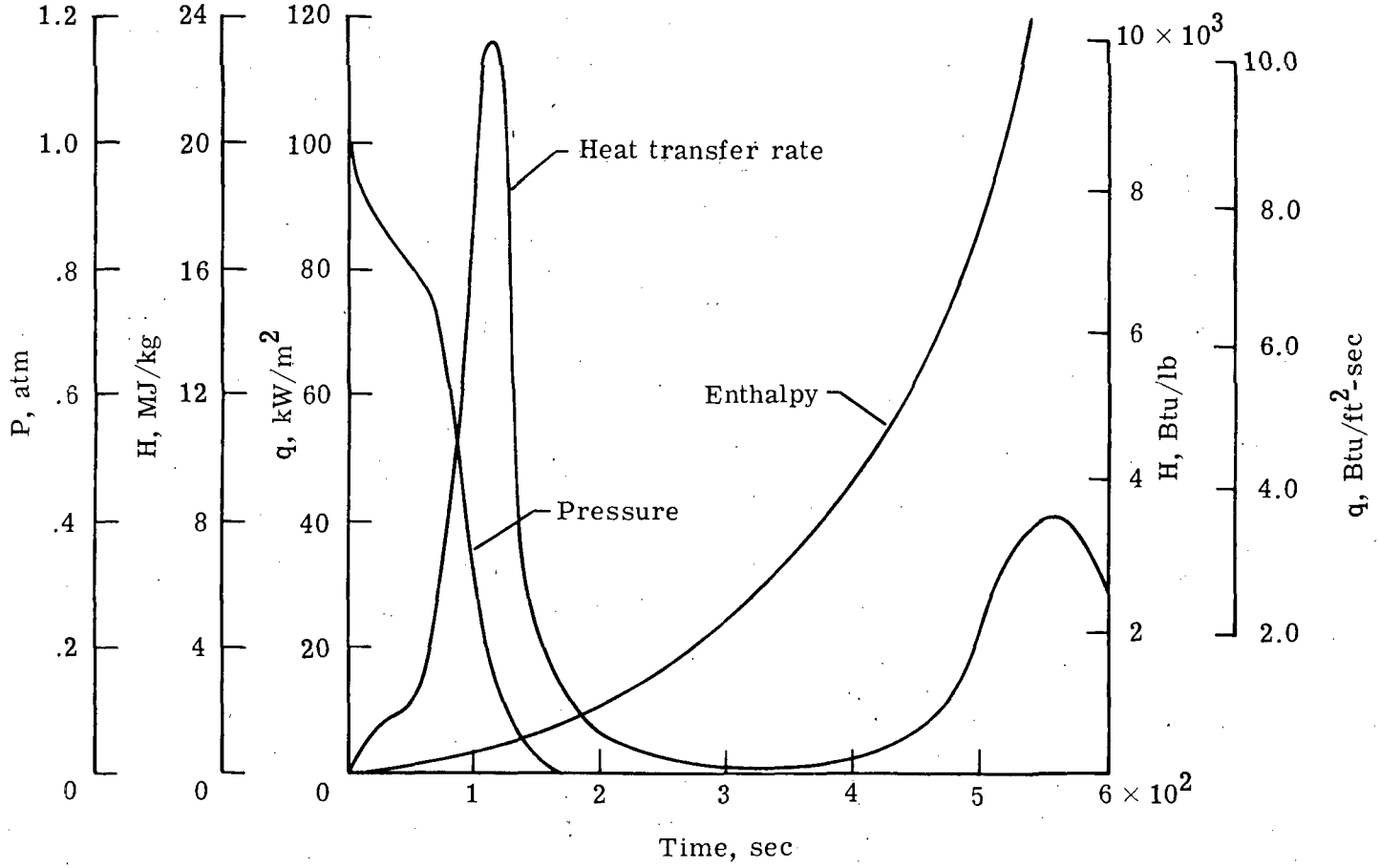

Figure 2.- Flight environment at maximum heating rate point on liquid oxygen tank (wall temperature, 255 K (0° F)).

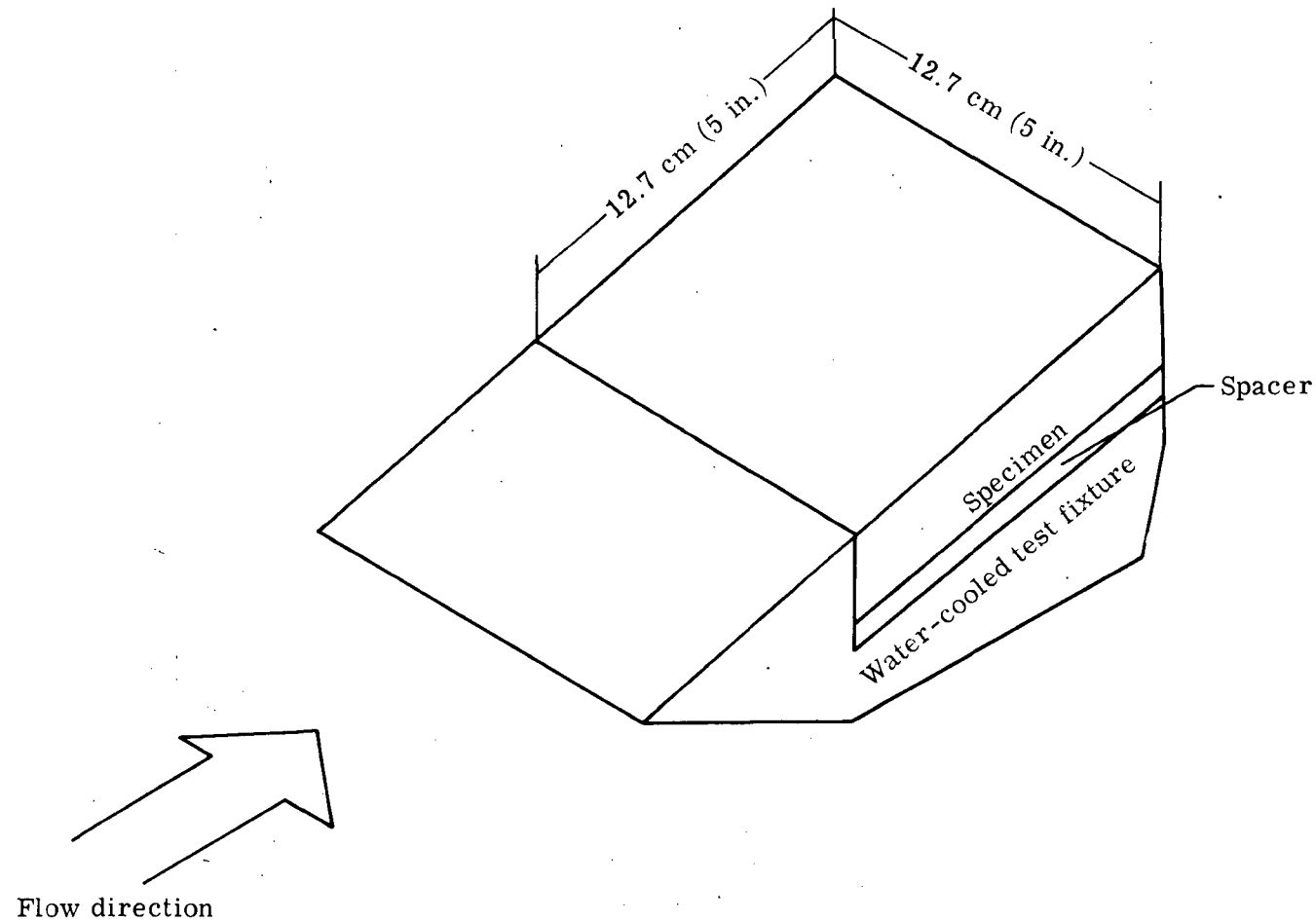

Figure 3.- Specimen mounted on test fixture.

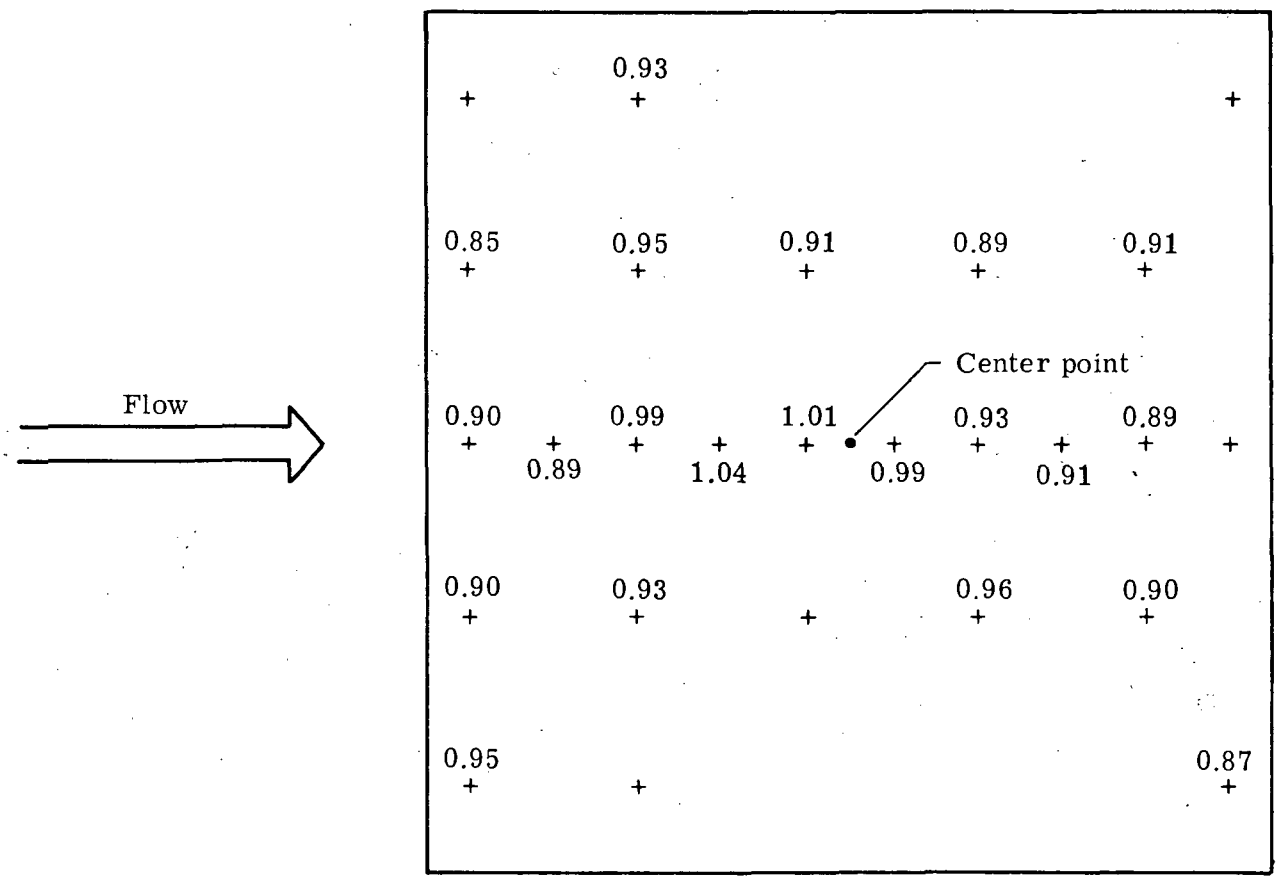

Figure 4.- Typical heating rate distribution (normalized to center point) for high enthalpy tests. Drawn to scale.

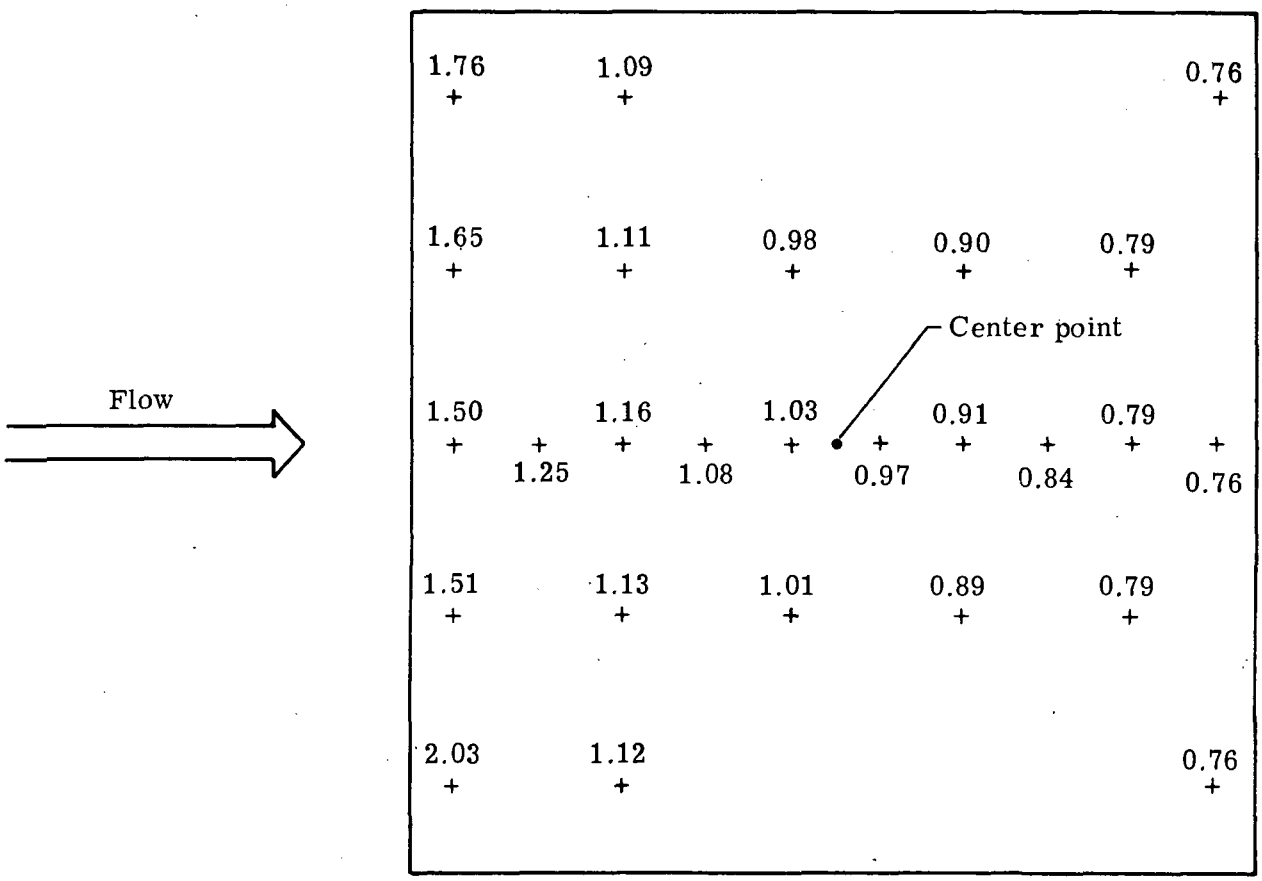

Figure 5.- Typical heating rate distribution (normalized to center point) for low enthalpy tests. Drawn to scale.

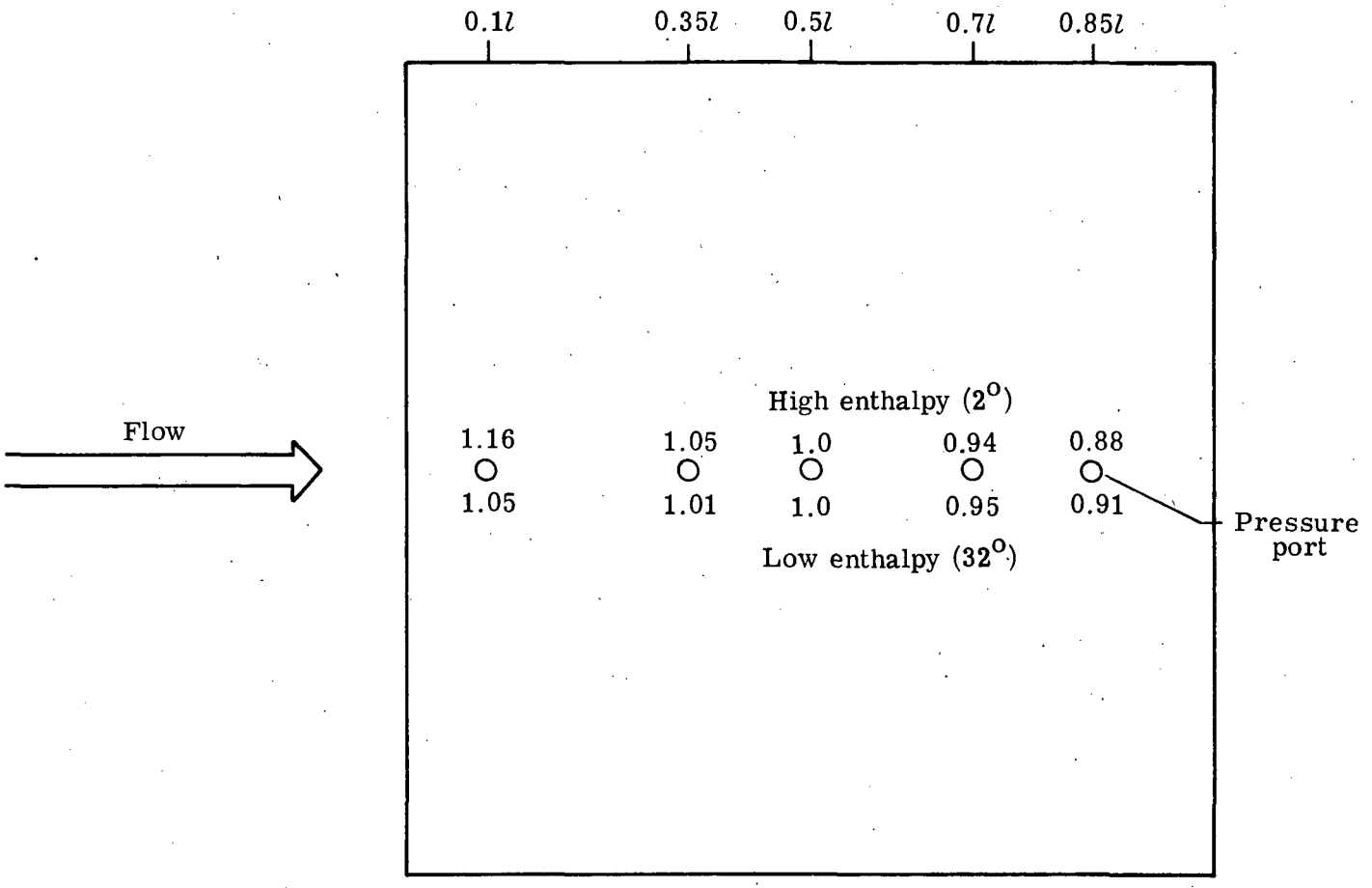

Figure 6.- Pressure port locations and typical pressure distributions (normalized to center point).

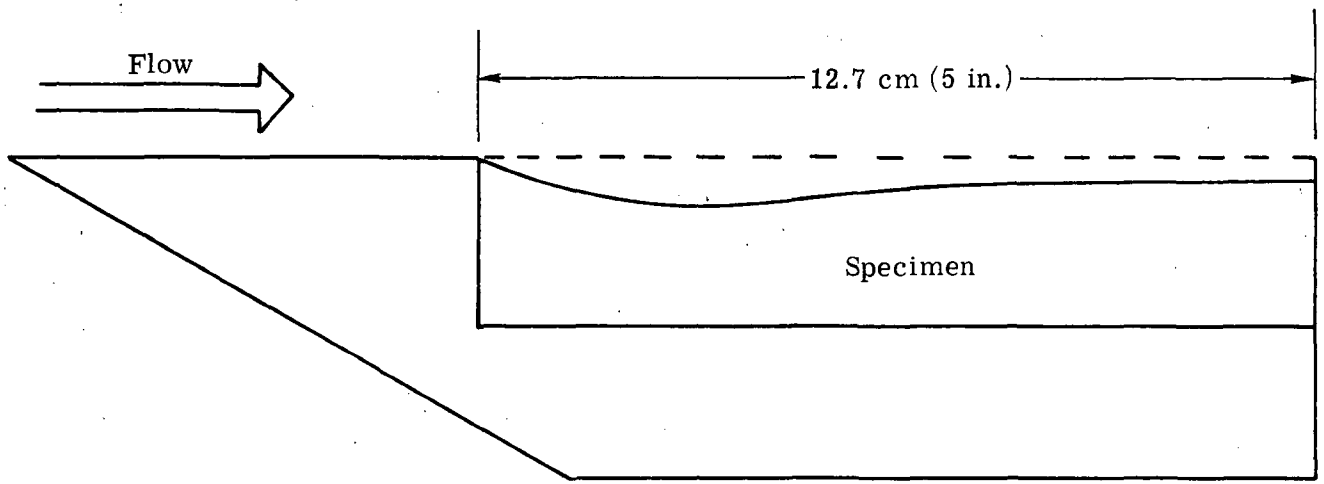

Figure 7.- Typical model shape after testing.

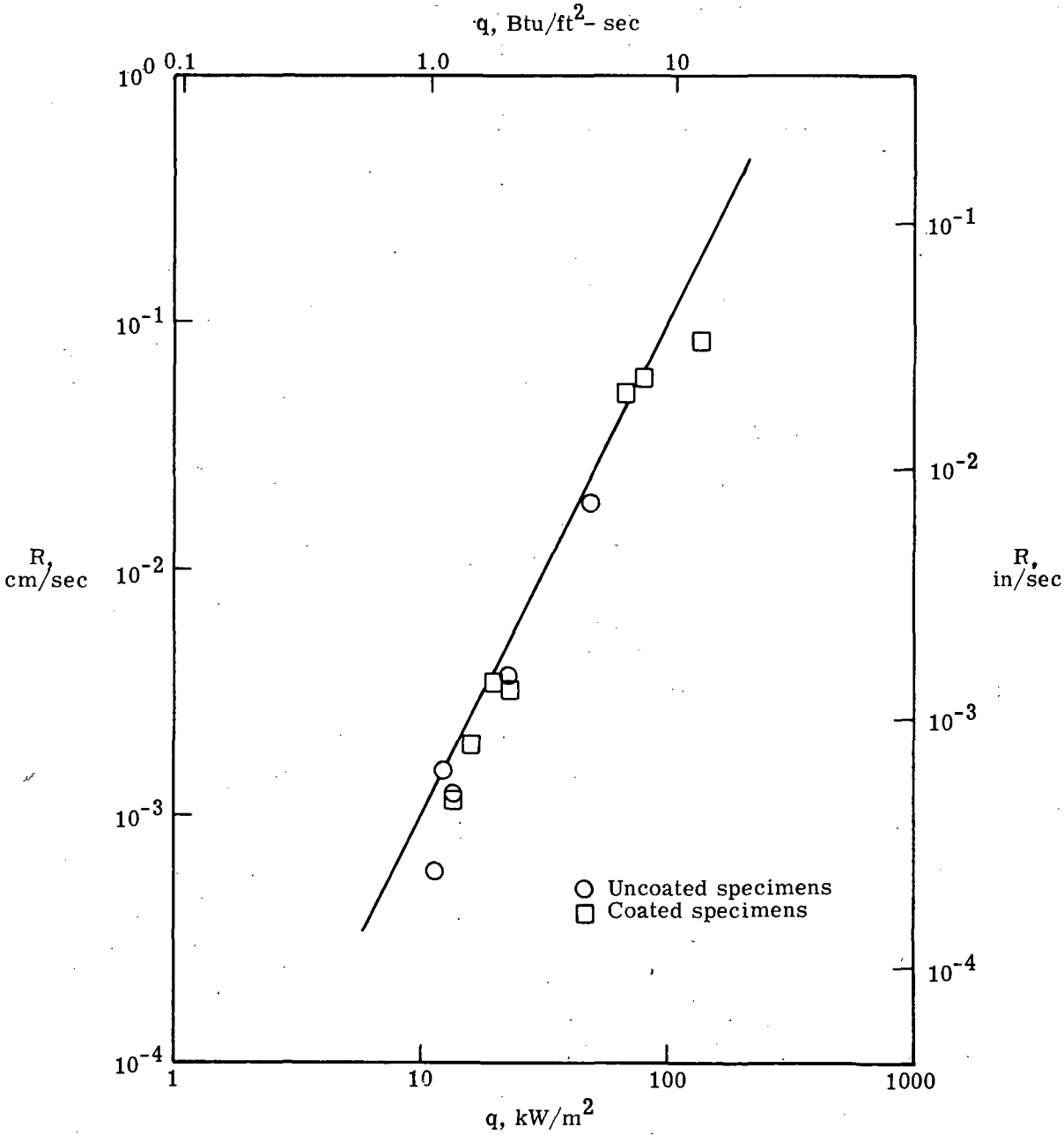

Figure 8.- Recession rate as a function of heating rate. High enthalpy tests.

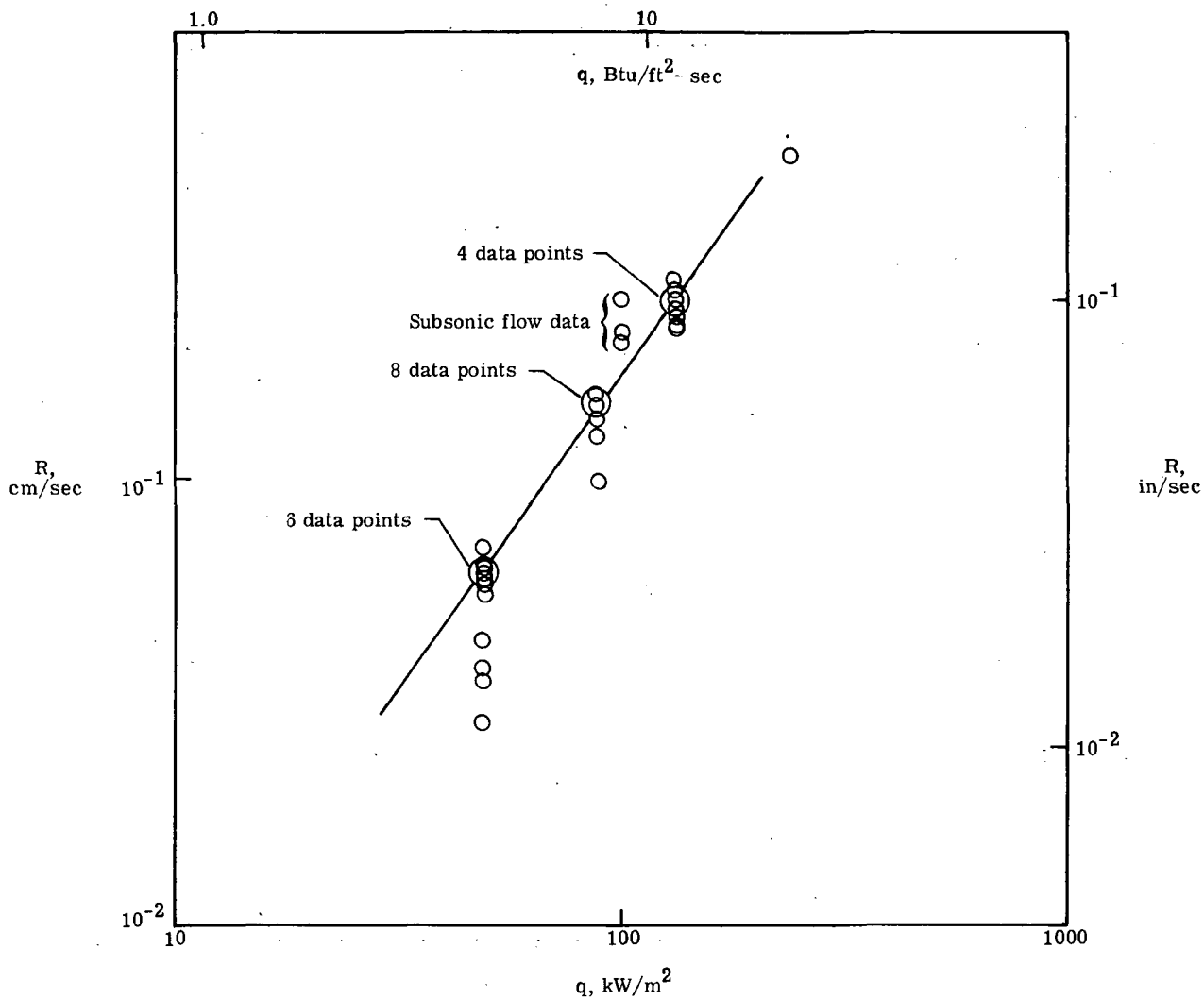

Figure 9.- Recession rate as a function of heating rate. Low enthalpy tests.

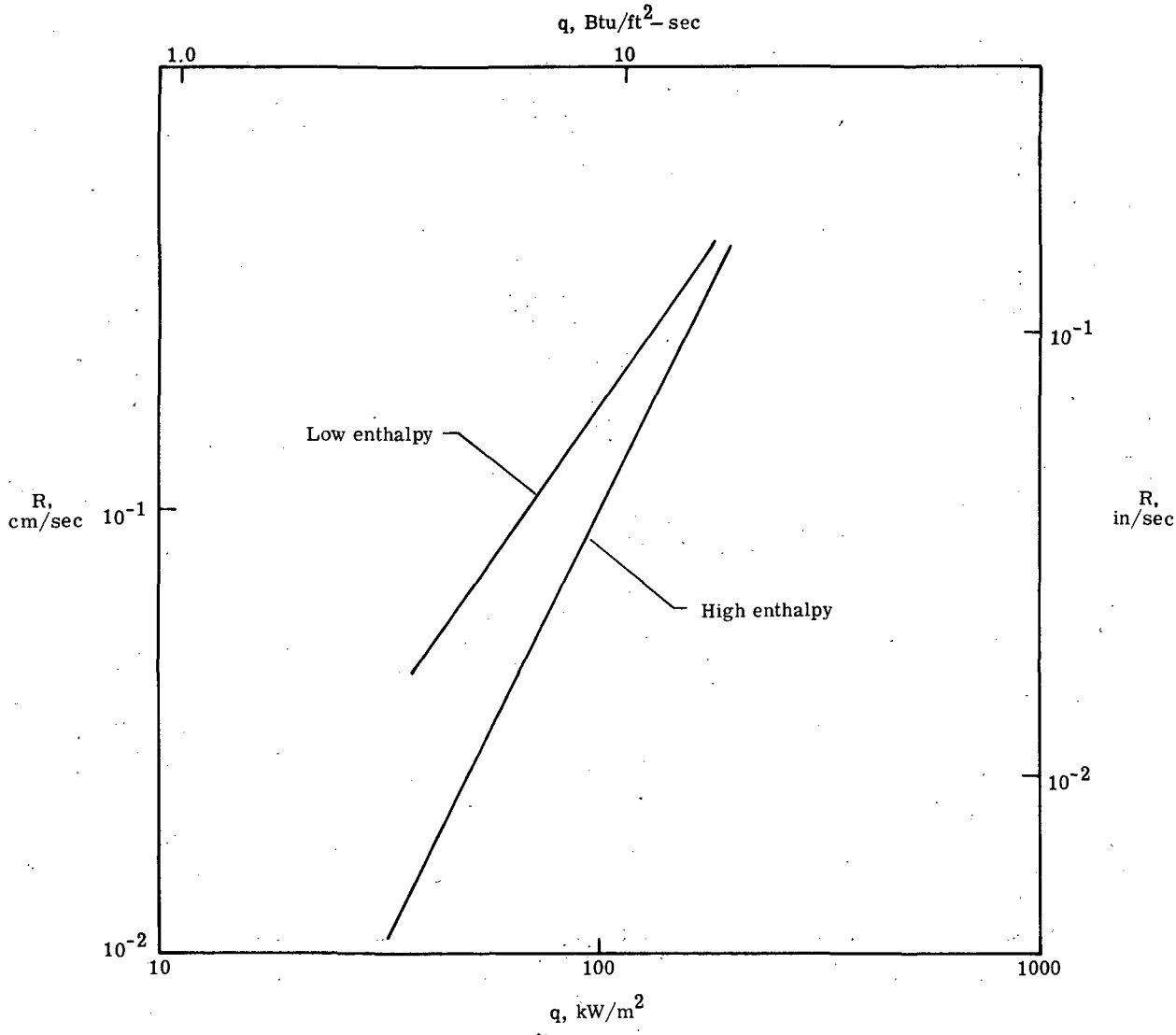

Figure 10.- High and low enthalpy curves.

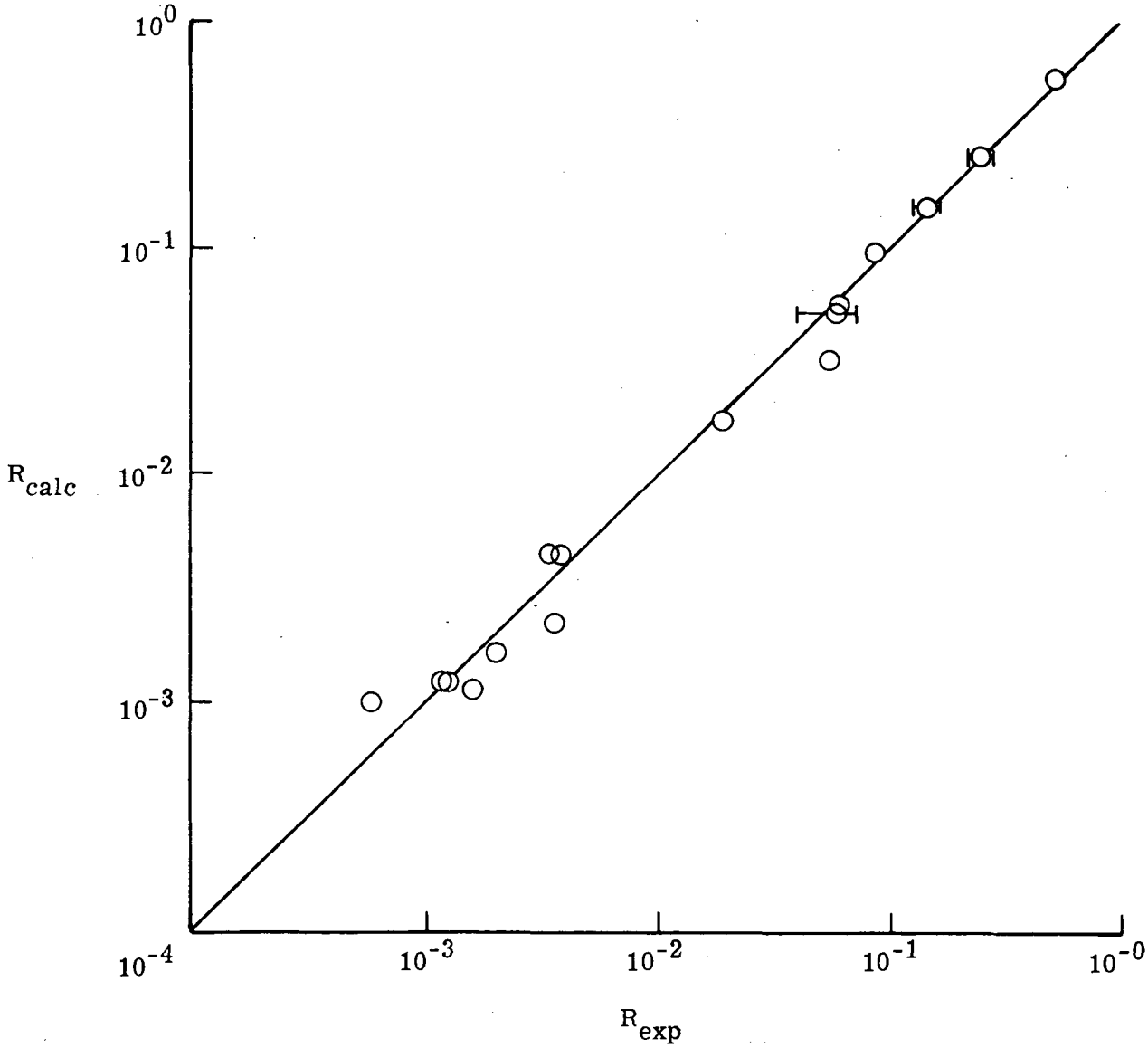

Figure 11.- Data correlation of calculated and experimental recession rates without subsonic, high pressure data.

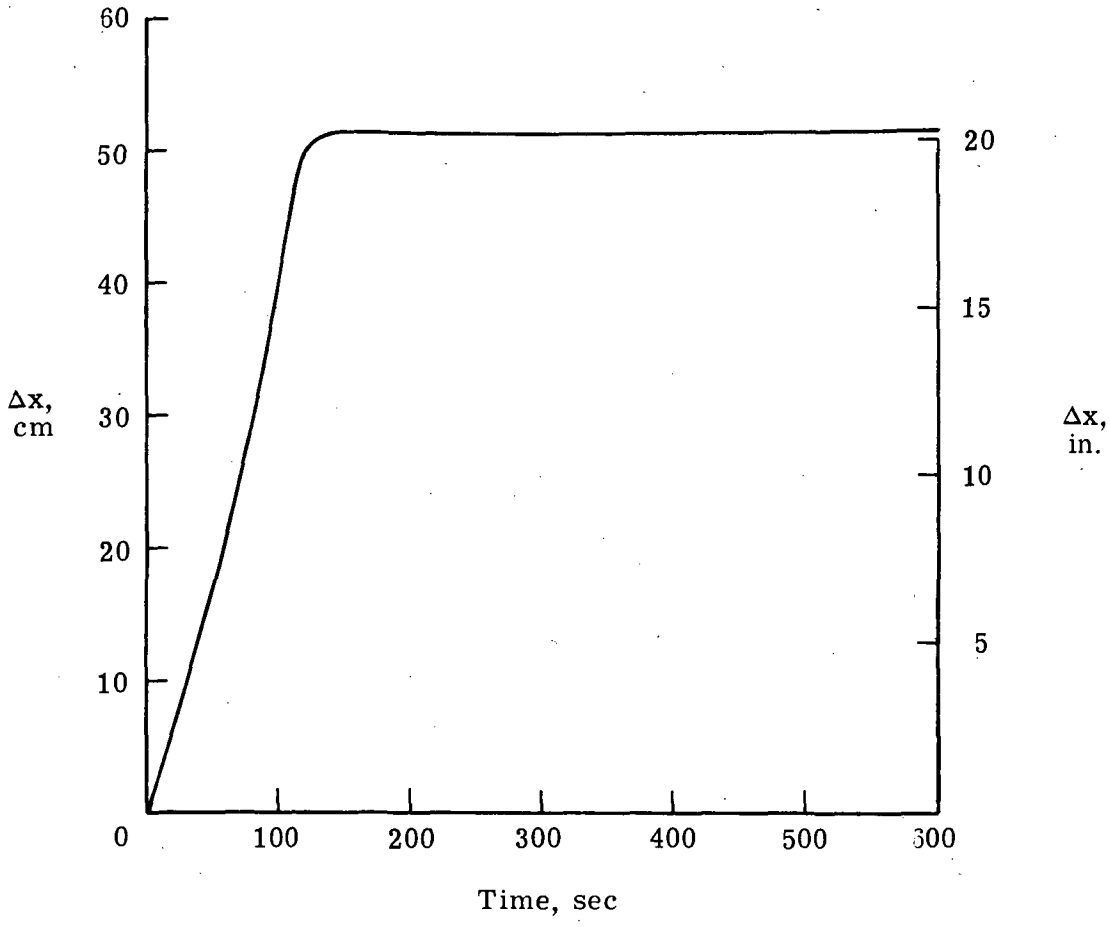

Figure 12.- Recession as a function of time for ascent trajectory. Correlation does not include subsonic, high pressure data.

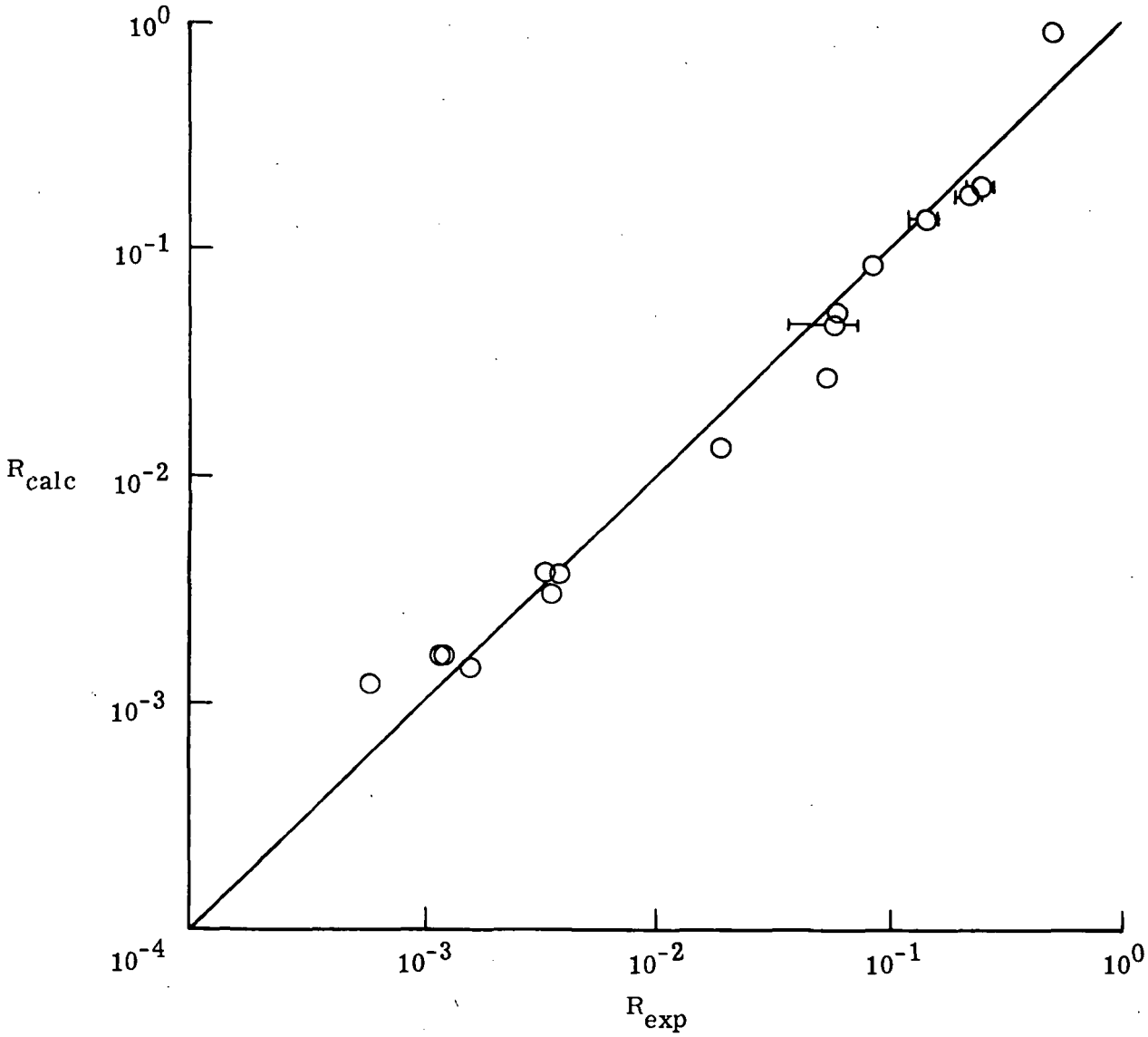

Figure 13.- Data correlation of calculated and experimental recession rates including subsonic, high pressure data. Unweighted.

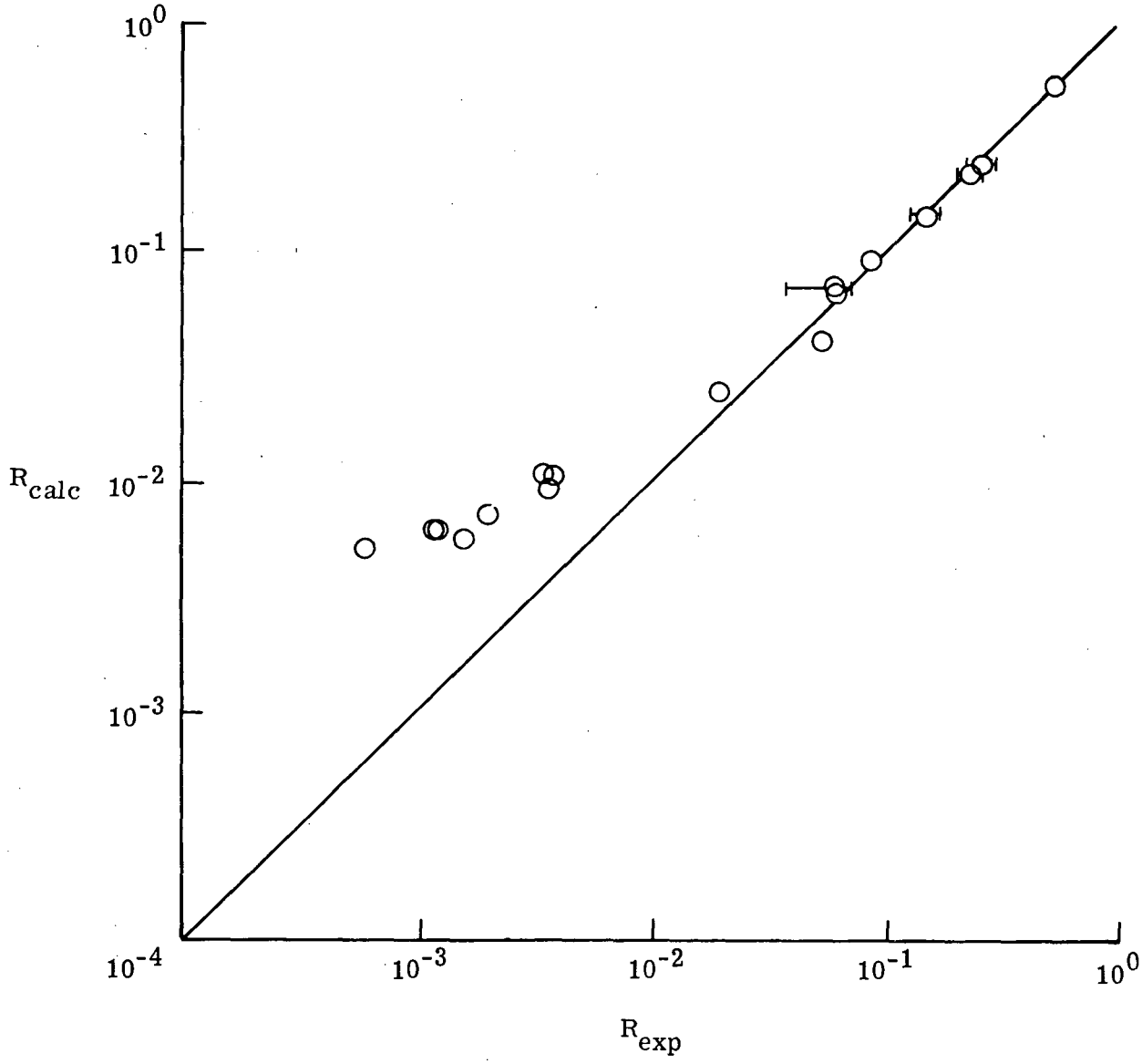

Figure 14.- Data correlation of calculated and experimental recession rates including subsonic, high pressure data. Weighted.

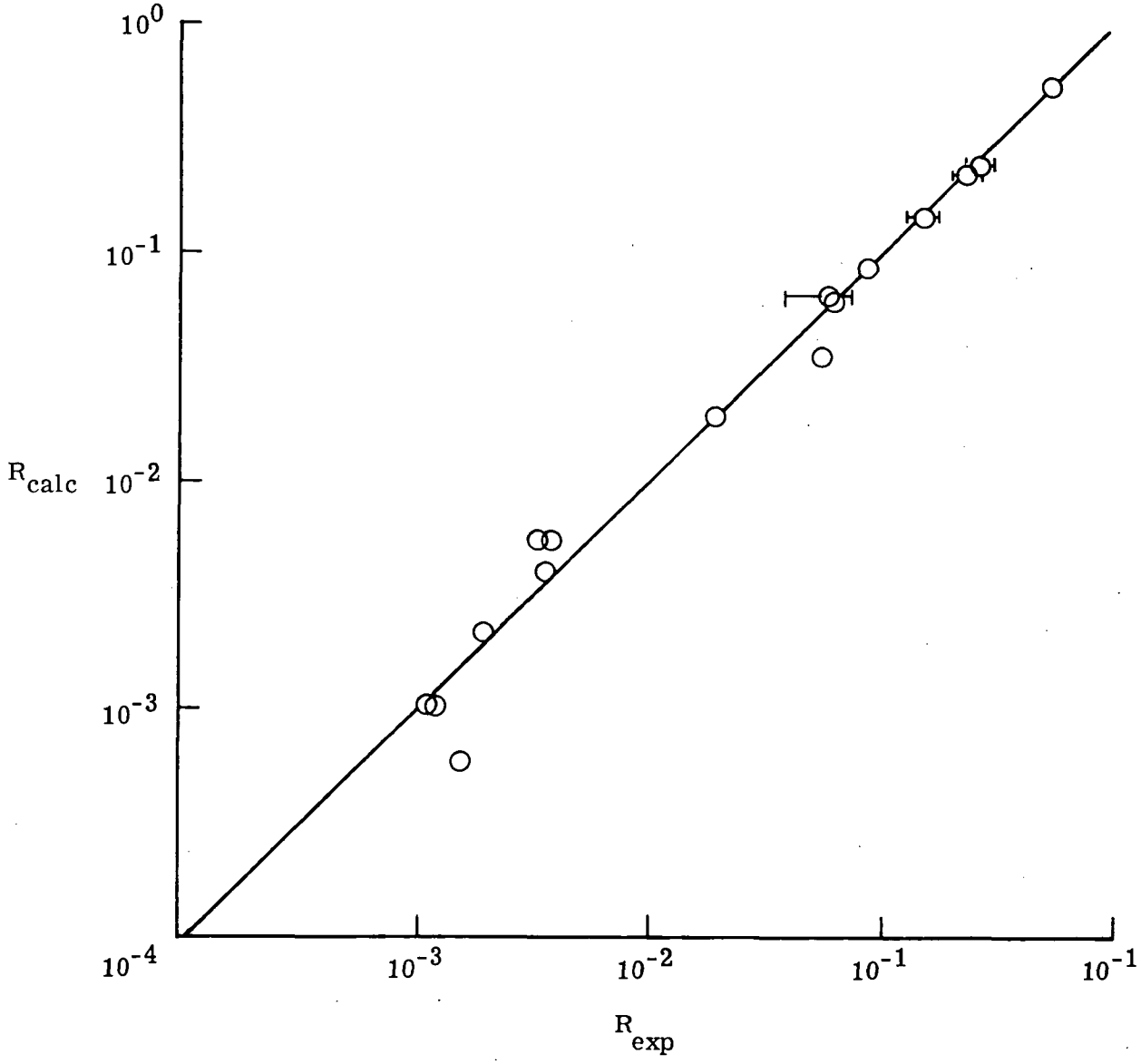

Figure 15.- Data correlation of calculated and experimental recession rates including subsonic, high pressure data. Weighted and modified.

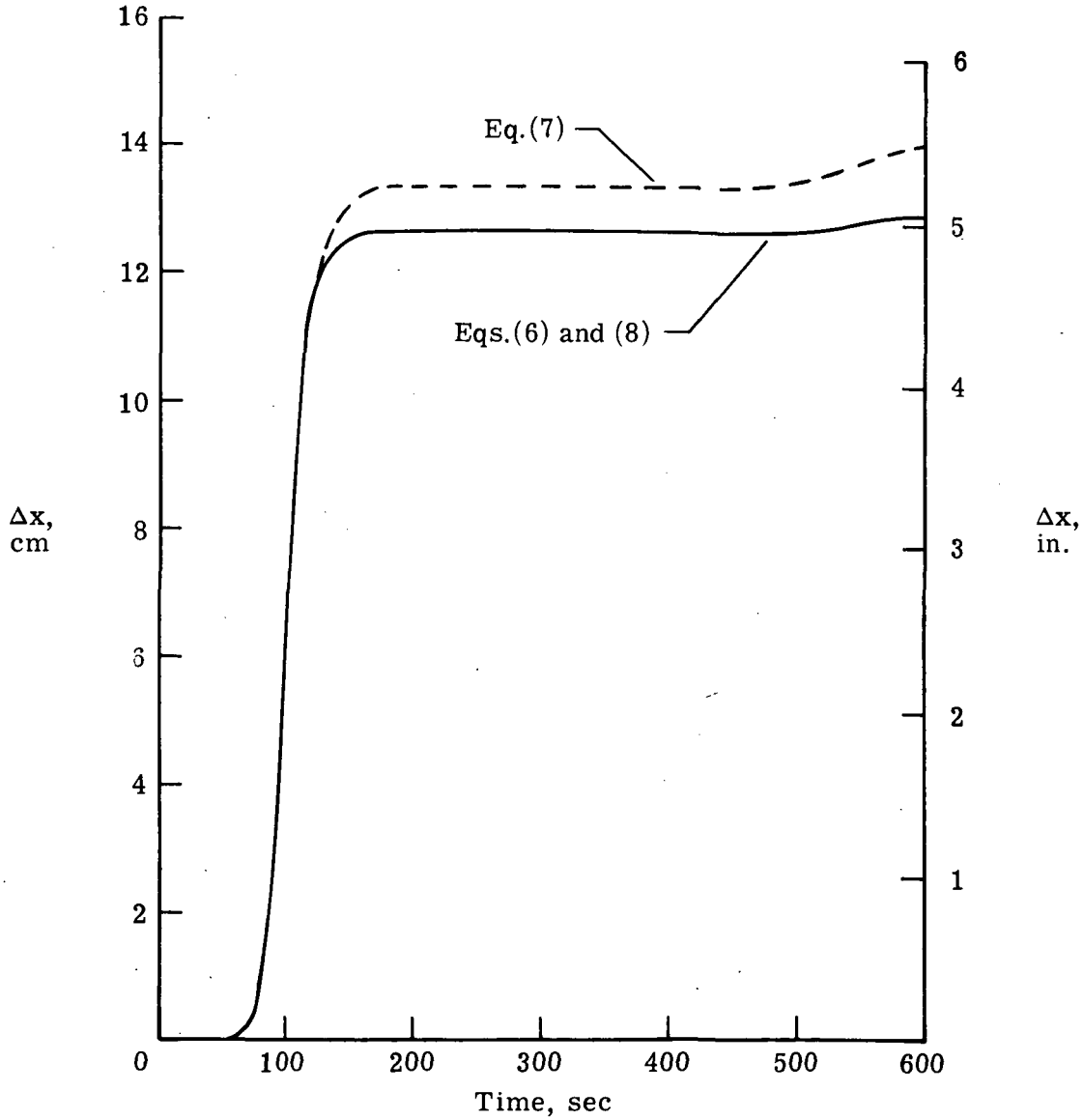

Figure 16.- Recession as a function of time for ascent trajectory. Correlations include subsonic, high pressure data.

"The aeronautical and space activities of the United States shall be conducted so as to contribute . . . to the expansion of human knowledge of phenomena in the atmosphere and space. The Administration shall provide for the widest practicable and appropriate dissemination of information concerning its activities and the results thereof."

—NATIONAL AERONAUTICS AND SPACE ACT OF 1958

NASA SCIENTIFIC AND TECHNICAL PUBLICATIONS

TECHNICAL REPORTS: Scientific and technical information considered important, complete, and a lasting contribution to existing knowledge.

TECHNICAL NOTES: Information less broad in scope but nevertheless of importance as a contribution to existing knowledge.

TECHNICAL MEMORANDUMS: Information receiving limited distribution because of preliminary data, security classification, or other reasons. Also includes conference proceedings with either limited or unlimited distribution.

CONTRACTOR REPORTS: Scientific and technical information generated under a NASA contract or grant and considered an important contribution to existing knowledge.

TECHNICAL TRANSLATIONS: Information published in a foreign language considered to merit NASA distribution in English.

SPECIAL PUBLICATIONS: Information derived from or of value to NASA activities. Publications include final reports of major projects, monographs, data compilations, handbooks, sourcebooks, and special bibliographies.

TECHNOLOGY UTILIZATION PUBLICATIONS: Information on technology used by NASA that may be of particular interest in commercial and other non-aerospace applications. Publications include Tech Briefs, Technology Utilization Reports and Technology Surveys.

Details on the availability of these publications may be obtained from:

SCIENTIFIC AND TECHNICAL INFORMATION OFFICE

NATIONAL AERONAUTICS AND SPACE ADMINISTRATION

Washington, D.C. 20546